ELSEVIER

Experimental Hematology

Experimental Hematology 2021;000:1–11

REGULAR SUBMISSION

Distinct effects of chondroitin sulfate on hematopoietic cells and the stromal microenvironment in bone marrow hematopoiesis

Takayuki Katagiri[a], Shun Uemura[a,b], Takashi Ushiki[a], Yaeko Nakajima-Takagi[b], Motohiko Oshima[b], Tadahisa Mikami[c], Asami Kawasaki[d], Hajime Ishiguro[a], Tomoyuki Tanaka[a], Hirohito Sone[a], Hiroshi Kitagawa[c], Michihiro Igarashi[d], Atsushi Iwama[b], and Masayoshi Masuko[e]

[a]*Department of Hematology, Faculty of Medicine, Niigata University, Niigata, Japan;* [b]*Division of Stem Cell and Molecular Medicine, Center for Stem Cell Biology and Regenerative Medicine, Institute of Medical Science, University of Tokyo, Tokyo, Japan;* [c]*Laboratory of Biochemistry, Kobe Pharmaceutical University, Kobe, Hyogo, Japan;* [d]*Department of Neurochemistry and Molecular Cell Biology, Graduate School of Medical and Dental Sciences, Niigata University, Niigata, Japan;* [e]*Department of Stem Cell Transplantation, Niigata University Medical and Dental Hospital, Niigata, Japan*

(Received 14 July 2020; revised 3 February 2021; accepted 7 February 2021)

The bone marrow (BM) microenvironment, known as the BM niche, regulates hematopoiesis but is also affected by interactions with hematopoietic cells. Recent evidence indicates that extracellular matrix components are involved in these interactions. Chondroitin sulfate (CS), a glycosaminoglycan, is a major component of the extracellular matrix; however, it is not known whether CS has a physiological role in hematopoiesis. Here, we analyzed the functions of CS in hematopoietic and niche cells. *CSGalNAcT1*, which encodes CS *N*-acetylgalactosaminyltransferase-1 (T1), a key enzyme in CS biosynthesis, was highly expressed in hematopoietic stem and progenitor cells (HSPCs) and endothelial cells (ECs), but not in mesenchymal stromal cells (MSCs) in BM. In T1 knockout (T1KO) mice, a greater number of HSPCs existed compared with the wild-type (WT), but HSPCs from T1KO mice showed significantly impaired repopulation in WT recipient mice on serial transplantation. RNA sequence analysis revealed the activation of IFN-α/β signaling and endoplasmic reticulum stress in T1KO HSPCs. In contrast, the number of WT HSPCs repopulated in T1KO recipient mice was larger than that in WT recipient mice after serial transplantation, indicating that the T1KO niche supports repopulation of HSPCs better than the WT niche. There was no obvious difference in the distribution of vasculature and MSCs between WT and T1KO BM, suggesting that CS loss alters vascular niche functions without affecting its structure. Our results revealed distinct roles of CS in hematopoietic cells and BM niche, indicating that crosstalk between these components is important to maintain homeostasis in BM. © 2021 Published by Elsevier Inc. on behalf of ISEH – Society for Hematology and Stem Cells.

In bone marrow (BM) hematopoiesis, it is well known that self-renewal, proliferation, and differentiation of hematopoietic stem and progenitor cells (HSPCs) are regulated by the microenvironment called the BM niche, which is affected by the interactions between hematopoietic cells and stromal cells. The BM niche consists mainly of two anatomically distinct cellular entities, the "endosteal niche" and the "vascular niche." HSPCs can move through these two regions and interact with the extracellular matrix (ECM) components [1]. Many studies have explored these

TK and MM designed the study, performed all experiments, and wrote the article. SU performed immunofluorescence imaging and FCM analysis of the BM niche cells. TU, AK, HI, and TT performed the BMTs. YNT, MO, and AI performed RNA sequencing. TM and HK performed HPLC quantification. MI and HS provided critical advice for performing the experiments and editing the article.

Offprint requests to: Masayoshi Masuko, Department of Stem Cell Transplantation, Niigata University Medical and Dental Hospital, 1-754 Asahimachi dori chuo-ku, Niigata 951-8520, Japan; E-mail: mmasuko@med.niigata-u.ac.jp

0301-472X/
https://doi.org/10.1016/j.exphem.2021.02.003

niches and their constituents, including cell adhesion molecules, growth factors, cytokines, and chemokines [2,3]. In contrast, recent studies have focused on the roles of ECM components in hematopoiesis. In particular, glycosaminoglycans (GAGs), known as major components of the ECM, are long linear polysaccharides of repetitive disaccharide sequences comprising an amino sugar moiety, synthesized by more than 10 glycosyltransferases and several sulfotransferases [4], and their significance in several hematopoietic processes has been revealed very recently.

For example, heparan sulfate (HS) and hyaluronic acid (HA) are known to modulate immune cell activities by binding to various signaling molecules, such as cytokines, chemokines, and growth factors [5–7]. In BM transplantation (BMT) experiments, mice heterozygous for *Ext1*, encoding an enzyme essential for HS synthesis [8,9], as recipient model mice (having stromal deficiency of HS), had a lower engraftment rate than WT recipients [10]. Similarly, conditional *Ext1* gene knockout (KO) in Mx1-expressing BM stromal cells (BMSCs) revealed HSPC mobilization from the BM to the spleen [11]. In hematopoietic systems, HA interacts with the CD44 molecule to promote HSC proliferation and differentiation [12,13].

Compared with HS and HA, the physiological roles of chondroitin sulfate (CS) in BM hematopoiesis or those in BMT are not directly analyzed. Similar to HS, CS chains are covalently linked to specific serine residues embedded in the core proteins via tetrasaccharide GAG-protein linkers and are found on numerous cell surfaces in the form of CS proteoglycans, including HSPCs and the BM stroma. HA also binds to versican, a member of the CS proteoglycans, to form the BM stroma, which controls the adhesion and migration of hematopoietic cells [14–16]. Therefore, CS chains are also thought to play key roles in ECM formation and HSC function; however, a good animal model for CS is needed.

We have postulated a CS-reduced mouse model, in which *CsGalNAcT1* encoding CS *N*-acetylgalactosaminyltransferase-1, the key enzyme for CS production, is deleted. Although *CSGalNAcT1* knockout (T1KO) mice have a body size 10% shorter than that of the WT because of the abnormal development of cartilage, they are viable to the adult stage and fertile with no other macroscopic changes [17]. In addition, they exhibit a 30%–50% reduction of CS synthesis [17–20], with microscopic abnormalities in perineuronal nets in the brain revealed by histochemical analysis. These results suggest that T1KO mice are a suitable model for analyzing the pathogenesis of human diseases resulting from reduced synthesis of CS [21].

In this study, we used T1KO mice to analyze the effects of CS on hematopoiesis. Although *CsGalNAcT1* loss did not have any significant effects other than a greater number of BM HSPCs on the steady state, HSPCs from T1KO mice exhibited impaired repopulation in WT recipient mice on serial transplantation. In contrast, the number of WT HSPCs repopulated in T1KO recipient mice was greater than that in WT recipient mice after serial transplantation, indicating that the T1KO BM niche supports repopulation of HSPCs better than the WT BM niche. As a result, we concluded that CS has distinct effects on hematopoietic cells and the BM stromal microenvironment in hematopoiesis.

Methods

Mice and BM transplantation procedure

CS *N*-acetylgalactosaminyltransferase-1 (*CsGalNAcT1*) knockout (T1KO) mice, which were previously described, were maintained on the C57BL/6 background [17]. C57BL/6-CD45.1 was provided by the RIKEN BRC through the National BioResource Project (NBRP) of the Ministry of Education, Culture, Sports, Science and Technology (MEXT), Japan. For transplantation, 8- to 10-week-old mice were subjected to 9 Gy irradiation [7,13] with a Cs irradiator using a PS-3000SB (Pony Industry Co., Ltd, Osaka, Japan) and were then injected with 3.0×10^6 BM mononuclear cells (MNCs), as previously described [22,23]. For serial transplantation, 2.0×10^6 BM MNCs were transplanted into 8- to 10-week-old recipient mice (C57BL/6-CD45.1) after 9 Gy of irradiation. Competitor cells consisted of 2.0×10^6 C57BL/6-CD45.1 BM MNCs. Five million BM MNCs from primary engrafted recipients were injected into the next transplantation recipient (C57BL/6-CD45.1), which had been lethally irradiated (9 Gy) 12 weeks after the previous BMT.

Flow cytometry

Flow cytometric analyses were performed using a CytoFLEX instrument (Beckman Coulter, Brea, CA, USA). Cell sorting was performed on a FACSAria II system (BD Biosciences, Franklin Lakes, NJ, USA). Antibodies are described in the Supplementary File E1 (online only, available at www.exphem.org).

HPLC quantification

BM cells from 8- to 10-week-old mice were used for the quantification of CS in the BM. The method for preparation of BM cells is described in the Supplementary Methods (online only, available at www.exphem.org). CS analyses were conducted by enzymatic treatment and HPLC-based quantification, as previously described [24].

Quantitative real-time polymerase chain reaction

Total RNA was extracted from the brain, peripheral blood (PB) mature cells (neutrophils: $CD11b^+Gr\text{-}1^+$ cells, B cells: $B220^+$ cells, T cells: $CD3^+$ cells), and 1.0×10^4 LSK cells from 8-week-old WT mice. We performed quantitative real-time polymerase chain reaction (qPCR) analysis according to protocols described in the Supplementary Methods (online only, available at www.exphem.org).

RNA sequencing

BM LSK cells from 8-week-old WT and T1KO mice were isolated by cell sorting. Total RNA was extracted from WT and T1KO BM LSK cells, and sequencing was performed according to the protocols described in the Supplementary Methods (online only, available at www.exphem.org).

Statistical analysis

Results were analyzed using unpaired Student *t* tests. All data are presented as mean ± SD. A p value < 0.05 was considered statistically significant.

Ethics statement

All animal experiments conducted in this study were performed with the approval of the Animal Experiment Committees of Niigata University. The approval number for the experiments is SA00217.

Data deposition

RNA sequencing data were deposited in the DNA Data Bank of Japan (Accession No. DRA009916).

Results

BM levels of CS disaccharides were lower in T1KO mice than in WT mice

We assessed the effects of CS on hematopoiesis using a CS-reduced mouse model, in which a gene encoding the rate-limiting CS-synthesizing enzyme, CS *N*-acetylgalactosaminyltransferase-1 (CSGalNAcT1), was disrupted. CS chains consist of repeating disaccharide units and are attached to core proteins to form CS proteoglycans (Figure 1A). Our results indicated that the BM levels of CS disaccharides in T1KO mice were approximately two-thirds of those in WT mice (Figure 1B). The chondroitin polymerase complex (CSGalNAcT1-indpendent pathway; Figure 1A) may exhibit polymerization activity only through combination of the two types of constituent enzymes. Hence, a single knockout of each enzyme does not easily affect the level of CS biosynthesis. However, the CSGalNAcT1-dependent pathway cannot be completely compensated for by other enzymes and, thus, is considered to be important for regulating CS levels even in BM.

RT-qPCR analysis of the brain, which enriches CS, and of BM LSK cells confirmed that the expression of *CSGalNAcT1* in LSK cells was approximately fourfold higher than that in the brain. In contrast, the expression of *CSGalNAcT1* in PB mature cells (neutrophils: $CD11b^+Gr\text{-}1^+$ cells, B cells: $B220^+$ cells, T cells: $CD3^+$ cells) was very low (Figure 1C). To further examine the expression of *CSGalNAcT1* in various compartments of the BM niche, we performed RT-qPCR for *CSGalNAcT1* in sinusoidal endothelial cells (sECs) and CXCL12-abundant reticular (CAR) cells. The expression of *CSGalNAcT1* was twofold higher in sECs than in LSK cells, whereas it was undetectable in CAR cells (Figure 1D). Therefore, our results suggest that CS disaccharides are abundant in HSPCs and sECs but not in CAR cells.

T1KO mice had significantly higher frequencies of BM HSPCs at the steady state

We first investigated the effect of CS reduction on hematopoiesis in the steady state. There were no significant differences in the numbers of PB cells (neutrophils, lymphocytes, Hb and platelets) and total BM cells between WT and T1KO mice (Supplementary Figures E1A and E2A online only, available at www.exphem.org). Meanwhile, T1KO mice exhibited significantly higher frequencies of BM LSK cells compared with WT mice (WT: 0.213 ± 0.044%; T1KO: 0.282 ± 0.046%, $p < 0.01$) (Figure 2A). The numbers of CFU-GM in BM cells were also higher in the T1KO mice group (WT: 29.6 ± 3.60; T1KO: 45.4 ± 2.37, $p < 0.01$) (Figure 2B). The percentages of LSK cells in the G0 phase were comparable for WT and T1KO mice (Figure 2C). There were no differences in CD44 expression levels in LSK cells between WT and T1KO mice (Figure 2D).

There are no obvious differences in the components of the BM niche in WT and T1KO mice

To evaluate the impact of *CSGalNAcT1* knockout on BM niche cells, we analyzed BM endothelial cells (ECs: $CD45^-$, $Ter119^-$, $CD31^+$, $CD144^+$) and mesenchymal stromal cells (MSCs: $CD45^-$, $Ter119^-$, $CD31^-$, $CD144^-$, $CD51^+$, $Pdgfr\alpha^+$) by flow cytometric analysis (Figure 2E). We assessed sinusoidal ECs (sECs: $CD105^{hi}$, $Sca\text{-}1^{int}$), arteriolar ECs (aECs: $CD105^{int}$, $Sca\text{-}1^{hi}$), CAR cells ($LepR^+Sca\text{-}1^-$), and PαS MSCs ($Sca\text{-}1^+LepR^-$) . We found that the frequency of sECs in the BM was slightly, but significantly, decreased in T1KO mice. In contrast, the frequencies of aECs, CAR cells, and PαS MSCs tended to increase, although the difference was not statistically significant (Figure 2E, F). To further assess the histologic properties of the niche compartments, we performed immunofluorescence imaging of BM blood vessels and MSCs. Consistent with the above data, we found no obvious differences in the distribution of vasculature and MSCs between WT and T1KO mice (Figure 2G).

HSPCs in T1KO mice exhibited short-term reconstitution delays after stem cell transplantation

BMT experiments were conducted to verify the impact of CS reduction in hematopoietic cells on hematopoiesis. BM cells from WT or T1KO mice were transplanted into 8- to 10-week-old recipient WT mice irradiated with a dose of 9 Gy. Hematopoiesis was evaluated at 5 weeks after BMT (Figure 3A). CS reduction in hematopoietic cells resulted in a smaller number of BM cells (Figure 3B), LSK HSPCs and

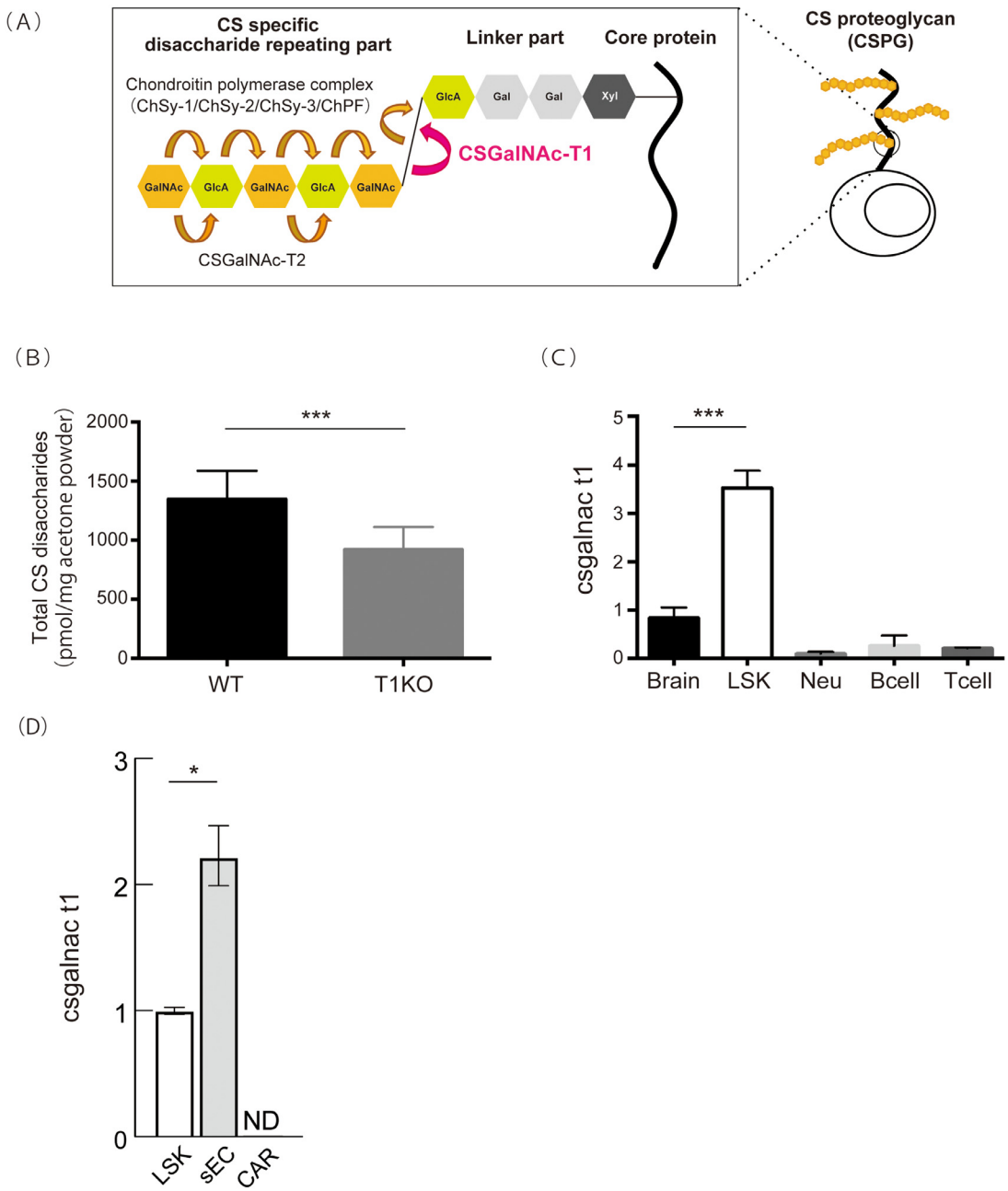

Figure 1. Expression levels of *CSGalNAcT1* are higher in HSPCs. **(A)** Schematic of CS proteoglycans and pathways of CS synthesis. CS chains are synthesized via two pathways: (1) *CSGalNAcT1*-dependent pathway—after the initial GalNAc transfer by *CSGalNAcT1*, the subsequent polymerization reaction proceeds mainly because of the chondroitin polymerase complex (chondroitin sulfate synthase: ChSy-1/ChSy-2/ChSy-3/chondroitin polymerizing factor: ChPF) and CSGalNAcT2; (2) *CSGalNAcT1*-independent pathway—chondroitin polymerization takes place directly on the tetrasaccharide linker part. **(B)** The total BM CS disaccharides in 8- to 10-week-old WT mice and *CsGalNAcT1* (T1) KO mice, as analyzed by HPLC-based quantification assay (WT, $n = 15$; T1KO, $n = 15$). **(C)** Expression levels of *CSGalNAcT1* in BM LSK cells, PB mature cells (neutrophils: $CD11b^{+}Gr\text{-}1^{+}$ cells, B cells: $B220^{+}$ cells, T cells: $CD3^{+}$ cells), and the brains of 8- to 10-week-old WT mice measured by RT-qPCR. **(D)** Expression levels of *CSGalNAcT1* in sECs and CAR cells, measured by RT-qPCR, and compared with those of BM LSK cells. All experiments were performed in triplicate ($n = 3$). *Xyl*=xylose; *Gal*=galactose, *GlcA*=glucuronic acid; *GalNAc*=*N*-acetyl-D-galactosamine. Data are represented as mean ± SD. $*p < 0.05$. $***p < 0.001$.

$CD34^{-}$ LSK HSCs compared with the number of WT hematopoietic cells (Figure 3C). However, at 16 weeks post-BMT, there was no difference in hematopoietic recovery (Figure 3D,E).

HSPCs from T1KO mice exhibited lower long-term reconstructive functions

We conducted competitive repopulation assays to reveal the effects of CS reduction on long-term

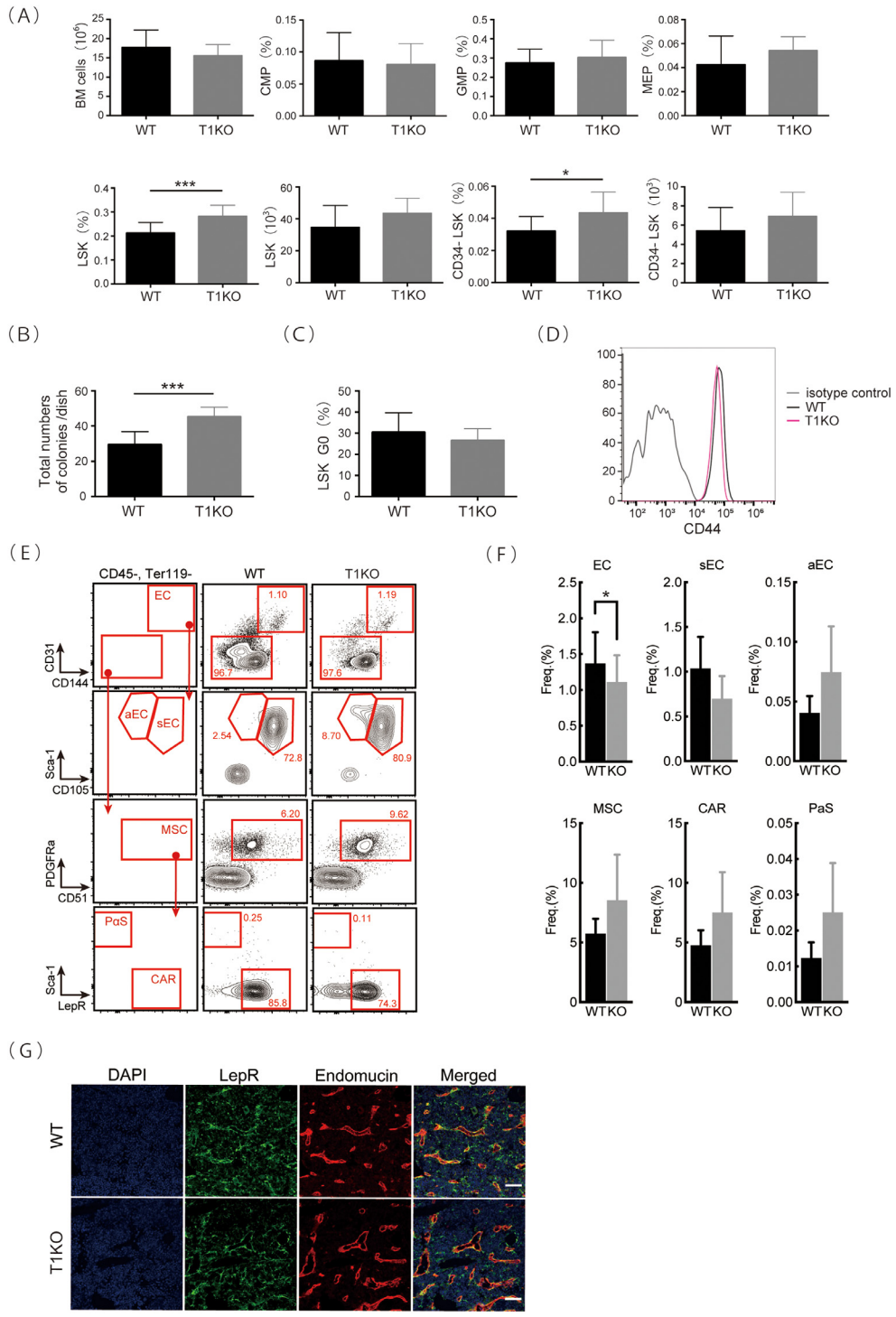

Figure 2. Percentages of HSPCs are higher in T1KO mice at steady state. **(A)** Hematopoietic analysis of 8- to 10-week-old WT and T1KO mice at steady state. Absolute numbers of BM cells and percentages of CMP cells (Lineage$^-$Sca-1$^-$c-Kit$^+$CD16/32^{Low}CD34$^+$), GMP cells (Lineage$^-$Sca-1$^-$c-Kit$^+$CD16/32^{High}CD34$^+$), MEP cells (Lineage$^-$Sca-1$^-$c-Kit$^+$CD16/32$^-$CD34$^-$), LSK cells, and CD34$^-$LSK cells in femurs are presented here (WT, n =15; T1KO, n = 15). **(B)** Total numbers of colonies (CFU-GM, CFU-G, and CFU-M) from BM cells (2.0×10^4) isolated from 8- to 10-week-old WT and T1KO mice and cultured in Methocult M3534 medium containing SCF, IL-3, and IL-6 (WT, n = 4; T1KO, n = 5). **(C)** Percentages of BM LSK cells in the G0 phase from 8- to 10-week-old WT and T1KO mice at steady state (WT, n = 7; T1KO, n = 7). **(D)** Histograms of CD44 expression in LSK cells of WT and T1KO mice. **(E)** Representative flow cytometric plots of ECs and MSCs in CD45$^-$Ter119$^-$ non-hematopoietic BM cells from WT and T1KO mice. **(F)** Frequencies of indicated cell types in the CD45$^-$Ter119$^-$ non-hematopoietic cell population (WT, n = 6; T1KO, n = 6). **(G)** Confocal imaging of BM sections from the femurs of 8- to 10-week-old WT and T1KO mice. Bar = 50 μm. Data are represented as mean ± SD, *$p < 0.05$. ***$p < 0.001$. *PαS*, Pdgfrα^+Sca1$^+$ cell.

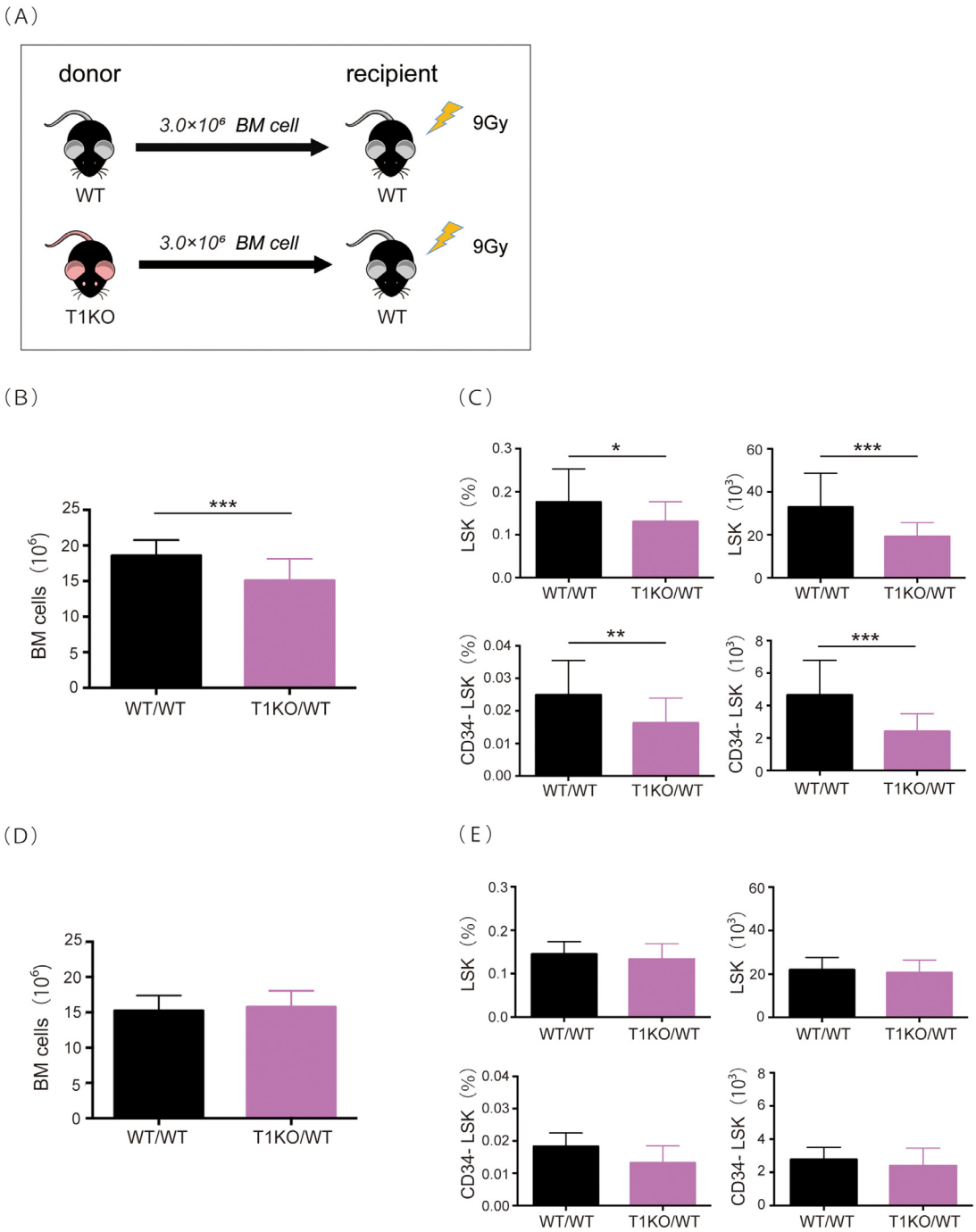

Figure 3. HSPCs in T1KO mice exhibited short-term reconstitution delay after stem cell transplantation. **(A)** Schematic of BM transplantation. BM cells from WT or T1KO mice were transplanted into 8- to 10-week-old recipient WT mice, which were irradiated at a dose of 9 Gy. Hematopoiesis was evaluated at 5 and 16 weeks post-BMT. **(B,C)** BM cells, LSK cells, and $CD34^-$ LSK cells in the femurs of each transplantation group at 5 weeks after BMT. (WT/WT, $n = 20$; T1KO/WT, $n = 19$). **(D,E)** BM cells, LSK cells, and $CD34^-$ LSK cells in femurs of each transplantation group 16 weeks after BMT (WT/WT, $n = 6$; T1KO/WT, $n = 6$). Data are represented as mean ± SD. $*p < 0.05$. $**p < 0.01$. $***p < 0.001$.

reconstructive functions of hematopoietic cells (Figure 4A). PB total cells, $Gr1^+CD11b^+$ cells, $B220^+$ cells, $CD3^+$ cells, and BM LSK cells were evaluated 6 and 12 weeks after each transplantation (Figure 4B–D). After the first transplantation, WT and T1KO donor cells did not exhibit significant differences in short-term reconstitution (after 6 weeks) and long-term reconstitution (after 12 weeks). However, after the secondary transplantation, hematopoietic cells derived from T1KO mice exhibited markedly lower chimerism across all lineages in PB cells. The

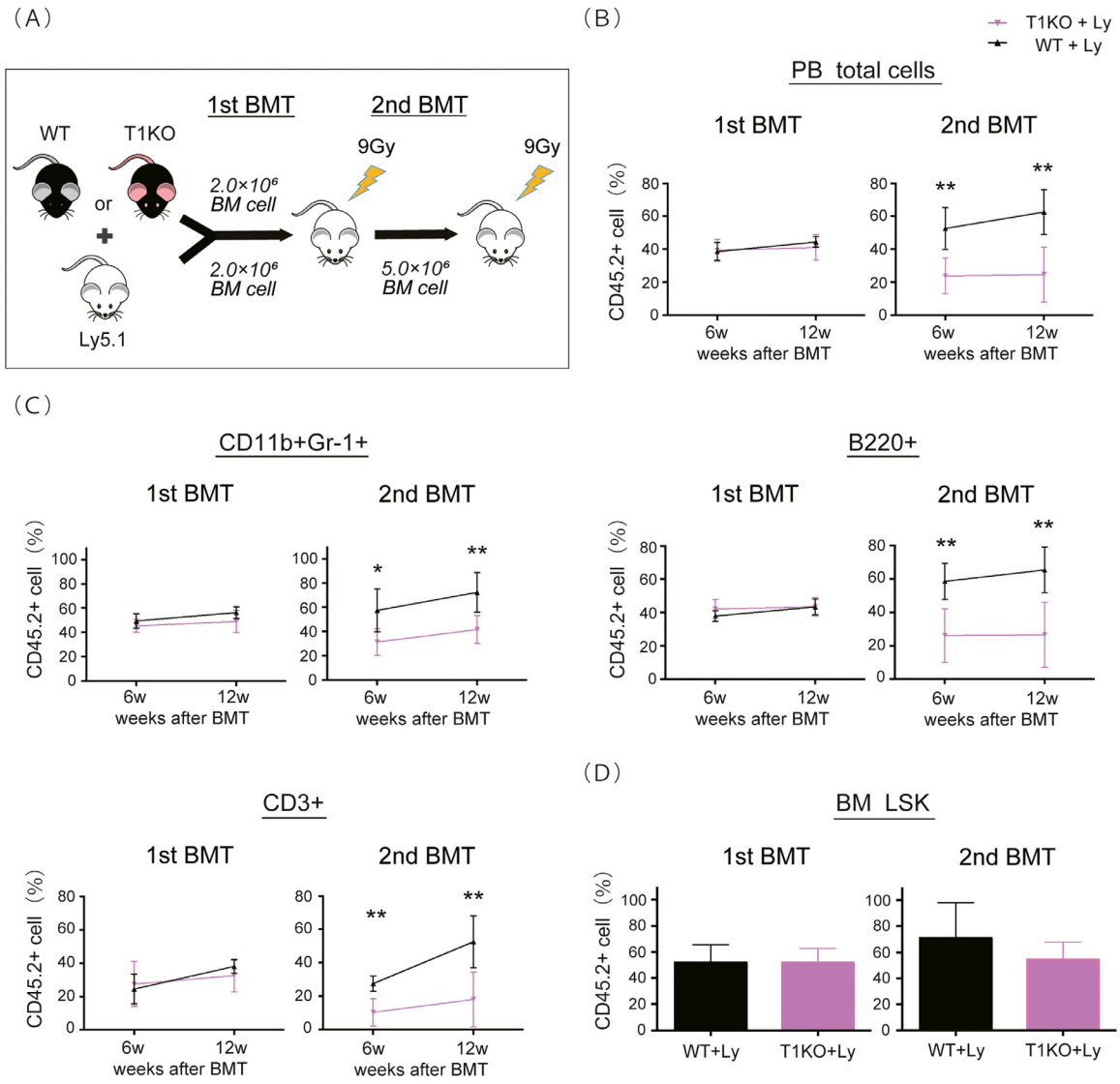

Figure 4. HSPCs from T1KO mice exhibited lower long-term reconstructive functions. **(A)** Schematic of a competitive repopulating unit CRU assay. BM cells (2.0×10^6) from WT or T1KO mice (CD45.2) were transplanted into 8- to 10-week-old recipient mice (CD45.1) irradiated at a dose of 9 Gy, together with 2.0×10^6 BM competitor cells from CD45.1 mice. For secondary transplantation, 5.0×10^6 BM cells were collected from all recipient mice 12 weeks posttransplantation and were then transplanted into 8- to 10-week-old CD45.1 mice irradiated at a dose of 9 Gy without competitor cells. **(B–D)** The chimerism of PB cells (PB total cells, Gr-1$^+$CD11b$^+$, B220$^+$, CD3$^+$) and BM LSK cells was analyzed 6 and 12 weeks after each transplantation (first transplantation: $n = 6$, second transplantation: $n = 6$). Data are represented as mean ± SD, $^*p < 0.05$. $^{**}p < 0.01$. $^{***}p < 0.001$.

chimerism of T1KO-derived cells in BM LSK cells also exhibited lower chimerism than WT cells after secondary transplantation, albeit with no statistical significance.

HSPC retention in T1KO niche after serial transplantations

To evaluate the effect of CS reduction in the BM niche on hematopoiesis, we performed serial transplantations (Figure 5A). BM cells from CD45.1 mice were transplanted into WT and T1KO recipient mice. The numbers of BM cells were found to decrease with serial transplantations (Figure 5B). The numbers of LSK HSPCs and CD34$^-$ LSK HSCs repopulated in the T1KO BM niche were higher than those in the WT BM niche (Figure 5C). These results suggest that the T1KO BM niche supports repopulation of HSPCs better than the WT BM niche during serial transplantations.

CS reduction in hematopoietic stem cells results in an increased expression of genes associated with regulation of IFN-α/β and endoplasmic reticulum (ER) stress

We analyzed expression levels of various genes in BM LSK cells from 8-week-old WT and T1KO mice.

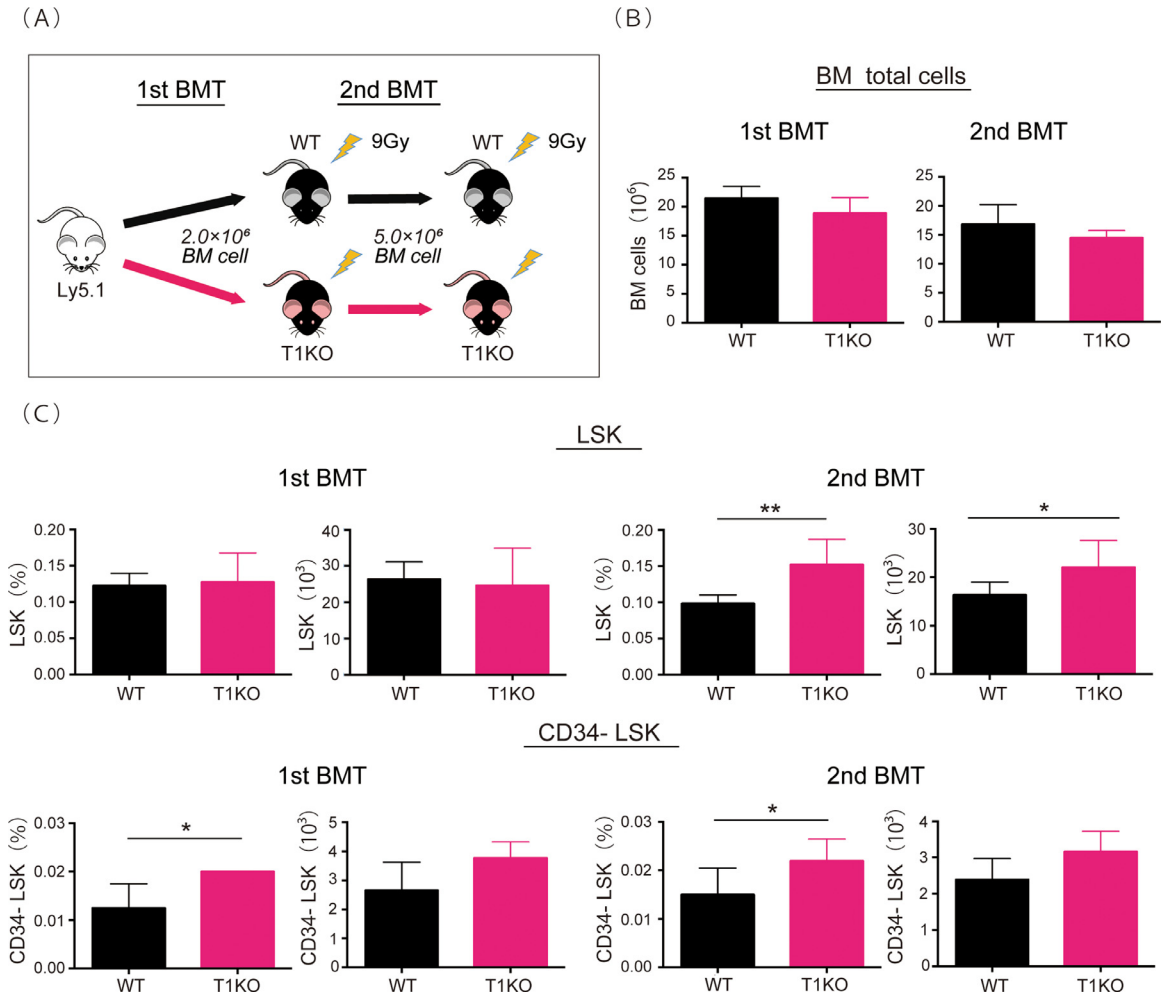

Figure 5. HSPCs were retained in the T1KO mice BM niche after serial transplantation. **(A)** Schematic of serial transplantation. BM cells (2.0×10^6) from CD45.1 mice were transplanted into 8- to 10-week-old recipient mice (WT or T1KO) irradiated at a dose of 9 Gy. For secondary transplantation, 5.0×10^6 BM cells were collected from all recipient mice at 12 weeks posttransplantation and were then transplanted into 8- to 10-week-old recipient mice (WT or T1KO) irradiated at a dose of 9 Gy. **(B,C)** BM cells, LSK cells, and $CD34^-$ LSK cells in femurs of each transplantation group were evaluated at 12 weeks posttransplantation (first transplantation: $n = 4$, second transplantation: $n = 6$). Data are represented as mean ± SD. *$p < 0.05$. **$p < 0.01$. ***$p < 0.001$.

Genes with significantly increased or decreased expression in T1KO LSK cells compared with that in WT LSK cells are indicated in the scatterplots (Figure 6A) and listed in Supplementary Table E1 (online only, available at www.exphem.org). Gene set enrichment analysis (GSEA) revealed that gene sets that are enhanced during ER stress were positively enriched in T1KO LSK cells ($p < 0.01$, false discovery rate [FDR] $q < 0.05$) (Figure 6B). Moreover, gene sets that are associated with IFN-α/β signaling were also markedly increased in T1KO LSK cells ($p < 0.01$, FDR $q < 0.01$) (Figure 6C). In addition, gene ontology (GO) analysis of the RNA-seq data revealed enrichment of genes in various biological processes, including developmental and metabolic processes, among the genes upregulated in T1KO LSK cells (Supplementary Figure 2A,B, online only, available at www.exphem.org).

Discussion

Our study found that HSPCs from T1KO mice had significantly impaired repopulation in WT recipient mice. In contrast, the number of WT HSPCs repopulated in T1KO recipient mice was greater than that in WT recipient mice after BM serial transplantation. These results clearly indicate that CS plays some physiological roles in hematopoiesis in both HSPCs and the BM niche.

Our results indicated that the level of CS disaccharides present in the BM of T1KO mice was approximately two-thirds of that in WT mice (Figure 1B). In contrast, the level of CS disaccharides in the cartilage and brain of T1KO mice was about half of that in WT mice [17,25]. These findings suggest that the contribution of the *CSGalNAcT1*-dependent pathway varies from tissue to tissue. We found that the expression level of *CSGalNAcT1* in BM LSK cells was very high

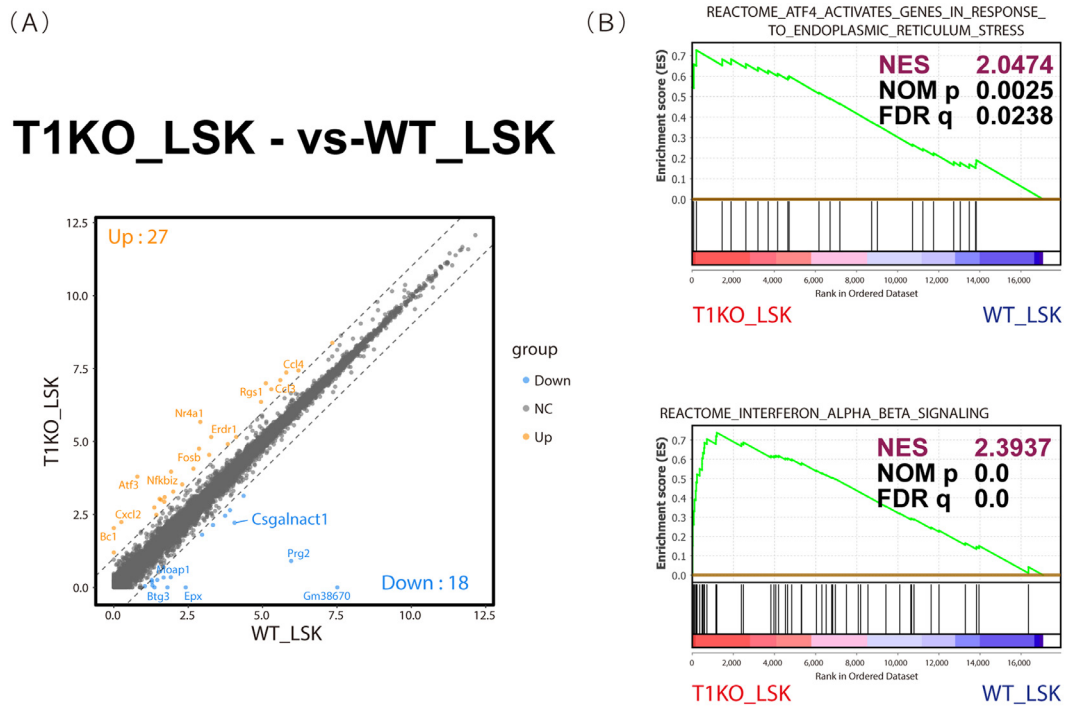

Figure 6. CS reduction in HSPCs results in increased expression of genes associated with regulation of IFN-α/β and ER stress. GSEA of T1KO and WT mice LSK cells (WT, $n = 2$; T1KO, $n = 2$). **(A)** Scatterplots of gene sets. The *x*- and *y*-axes indicate log-scaled fragments per kilobase of transcript per million (FPKM) of T1KO LSK and WT LSK groups, respectively. *Gray dots* represent no change (NC) genes, *orange dots* represent genes upregulated in T1KO LSK, and *blue dots* represent the genes that are downregulated. **(B,C)** GSEA of ER stress and regulation of IFN-α/β gene sets for T1KO LSK cells compared with WT LSK cells.

(Figure 1C), suggesting that immature hematopoietic cells are richer in CS disaccharides than mature ones. Previous reports indicated that CS and HS are also expressed in embryonic stem cells (ESCs) and play crucial roles in maintaining mouse ESCs [4]. In undifferentiated mouse ESCs, HS accounts for approximately 80% of the total GAGs and CS accounts for the rest (approximately 20%) [9,26,27] CS and HS are important for ESC self-renewal and differentiation, and it is known that their expression levels change when ESCs differentiate into EBs and/or more specific lineages [26–28]. The present data, together with previous reports on HS, suggest that CS and HS are also important for HSC self-renewal and differentiation and that their expression levels change when HSCs differentiate into mature cells.

Except for the greater number of BM HSPCs in hematopoiesis during the steady state, *CSGalNAcT1* KO did not have any significant effects. However, HSPCs in T1KO mice exhibited short-term reconstitution delays after stem cell transplantation (Figure 3B, C). Although these differences in hematopoietic recovery had disappeared 16 weeks post-BMT (Figure 3D, E), competitive repopulation assays clearly revealed that hematopoietic cells derived from T1KO mice exhibited markedly lower chimerism than WT cells across all lineages of PB cells during secondary transplantation (Figure 4B,C). These results revealed reduced repopulating capacity of T1KO HSCs. These findings were similar to those of *Ext-1* KO models, where the major enzyme that synthesizes heparan sulfate (HS) was abolished [10,11].

In contrast, the number of HSPCs repopulated in the T1KO BM niche was greater than that in the WT BM niche after serial transplantation (Figure 5C). These results suggest that the T1KO BM niche supports the repopulation of HSPCs better than the WT BM niche. Mild hematopoietic changes in T1KO mice could be attributed to mild reductions of CS disaccharides in the BM of T1KO mice, as illustrated in Figure 1B. Therefore, CS in the BM niche may inhibit the retention of HSPCs. This hypothesis is consistent with a previous report indicating that CS inhibits the regeneration of central nerve cells [18].

The expression of *CSGalNAcT1* was two times higher in sECs than in LSK cells but not detectable in CAR cells, suggesting active CS synthesis in endothelial niche cells (Figure 1D). Although the frequency of sECs was mildly decreased in T1KO mice, there were no obvious differences in the distribution of vasculature and MSCs between WT and T1KO mice according to immunofluorescence imaging of BM blood vessels

and MSCs (Figure 2G). These results collectively demonstrate that T1KO may alter the function of the vascular niche without affecting its structure.

Various molecules are known to be involved in the maintenance of the BM niche. Interaction between HSC and HA via CD44 is one of the major regulatory mechanisms for HSC proliferation and differentiation [12,13]. HSCs bind to HA minimally at the steady state; these bindings are strengthened when HSCs are induced to proliferate. On the other hand, HPCs have a high affinity for HA at the steady state, and the interactions between HSPCs and HA promote cell proliferation [13]. CD44 is known to suppress the ability of HSPCs to bind to HA in vitro via CS glycosylation [29]. Although most of the CS proteoglycans on hematopoietic cells seem to be related to CD44, we found no differences in CD44 expression levels between WT and T1KO mouse LSK cells using an anti-CD44 antibody that recognizes an epitope common to alloantigens and all isoforms (Figure 2D) [30,31]. Therefore, our findings suggest that the differences in LSK cell function in T1KO mice result from CS reduction even if CD44 expression remains the same.

In RNA-seq analysis, the expression of genes associated with ER stress was found to be upregulated in LSK cells from T1KO mice compared with that in WT mice (Figure 6B). Interactions between CS chains and these receptors intracellularly activate RhoA signaling and inactivate the AKT and ERK pathways [32]. Therefore, CS reduction can lead to cell proliferation as a result of enhanced AKT and ERK signaling. HSCs are basically in a dormant state but are required for greater protein synthesis ability and folding capacity under proliferative conditions. Increased protein synthesis triggers ER stress and the unfolded protein response (UPR). Sustained activation of these processes is known to cause apoptosis of HSCs, so appropriate management of ER stress and UPR is crucial for maintaining HSCs [33–35]. The CS of HSPCs could be involved in the fine-tuning of these processes. In addition, we observed increased expression of genes associated with IFN-α/β signaling in T1KO mice (Figure 6C). It is known that HSCs exit the dormant state (G0 phase) and enter the cell cycle in response to IFN-α, resulting in increased phosphorylation of STAT1 and AKT1 and upregulation of stem cell antigen-1 (Sca-1) [36]. Conversely, it is also known that Akt-mTOR activation in endothelial cells, which are part of the BM niche, upregulates angiocrine factors that support self-renewal of long-term HSCs and expansion of HSPCs [37]. These findings suggest that the proliferation and activation of BM niche cells caused by CS reduction might contribute to the improvement of the repopulation abilities of HSPCs.

Previous studies have reported the functions of GAGs (e.g., HS, HA), primarily in the BM niche [10–16], and a few other reports related to the effects of GAGs on HSPCs themselves also exist [7,38]. GAG chains, especially HS, can bind humoral factors, such as cytokines, chemokines, growth factors, and morphogens, to present them to their receptors. In this context, GAG chains act as coreceptors or reservoirs for humoral factors [4,5]. In addition, CS chains can interact with cell surface receptor molecules on their own, and, therefore, function as extracellular signaling molecules that trigger CS-receptor–mediated signal transduction [4]. CS chains can be found on various cells in the form of CS proteoglycans, including the BM microenvironment and HSPCs. Several CS proteoglycans, such as versican [39], NG2 [40], SMC3 [41], serglycin [42], and CD44, are reported to be involved in hematopoiesis. Our data suggest that CS chains have an important role in the function of CS proteoglycans in BM hematopoiesis.

In conclusion, our present results suggest a unique effect of CS on hematopoietic cells and the BM niche. Crosstalk interactions between them are considered important in hematopoiesis. Manipulating the level of CS in HSPCs and in the BM niche may improve the outcome of clinical hematopoietic stem cell transplantation in the future.

Acknowledgments

This study was supported in part by Grants-in-Aid for Scientific Research (Grant No. 15K19547 to Dr. T Ushiki, Grant No. 19K08001 to Dr. H Ishiguro, Grant Nos. 18H04013 and 18H04670 to Dr. M Igarashi, and Grant No. 16K09868 to Dr. M Masuko), the Ministry of Education, Culture, Sports, Science, and Technology (MEXT) of Japan, the Japan Society of Promoting Sciences (JSPS), a Japanese Society of Hematology Research Grant (2018–2019) to Dr. M Masuko, and Advanced Research & Development Programs for Medical Innovation AMED–CREST grants (Grant Nos. 19gm1210007s0101 and 20gm1210007s0102 to Dr. M Igarashi) from AMED (Japan Agency for Medical Research and Development).

References

1. Gattazzo F, Urciuolo A, Bonaldo P. Extracellular matrix: a dynamic microenvironment for stem cell niche. Biochim Biophys Acta. 2014;1840:2506–2519.
2. Shiozawa Y, Havens AM, Pienta KJ, Taichman RS. The bone marrow niche: habitat to hematopoietic and mesenchymal stem cells, and unwitting host to molecular parasites. Leukemia. 2008;22:941–950.
3. Boulais PE, Frenette PS. Making sense of hematopoietic stem cell niches. Blood. 2015;125:2621–2629.
4. Mikami T, Kitagawa H. Sulfated glycosaminoglycans: their distinct roles in stem cell biology. Glycoconj J. 2017;34:725–735.
5. Papy-Garcia D, Albanese P. Heparan sulfate proteoglycans as key regulators of the mesenchymal niche of hematopoietic stem cells. Glycoconj J. 2017;34:377–391.
6. Viviano BL, Silverstein L, Pflederer C, Paine-Saunders S, Mills K, Saunders S. Altered hematopoiesis in glypican-3-deficient

mice results in decreased osteoclast differentiation and a delay in endochondral ossification. Dev Biol. 2005;282:152–162.
7. Khurana S, Margamuljana L, Joseph C, Shouteden S, Buckley SM, Verfaillie CM. Glypican-3-mediated inhibition of CD26 by TFPI: a novel mechanism in hematopoietic stem cell homing and maintenance. Blood. 2013;121:2587–2595.
8. Lin X, Gan L, Klein WH, Wells D. Expression and functional analysis of mouse EXT1, a homolog of the human multiple exostoses type 1 gene. Biochem Biophys Res Commun. 1998;248:738–743.
9. Lin X, Wei G, Shi Z, et al. Disruption of gastrulation and heparan sulfate biosynthesis in EXT1-deficient mice. Dev Biol. 2000;224:299–311.
10. Shekels LL, Buelt-Gebhardt M, Gupta P. Effect of systemic heparan sulfate haploinsufficiency on steady state hematopoiesis and engraftment of hematopoietic stem cells. Blood Cells Mol Dis. 2015;55:3–9.
11. Saez B, Ferraro F, Yusuf RZ, et al. Inhibiting stromal cell heparan sulfate synthesis improves stem cell mobilization and enables engraftment without cytotoxic conditioning. Blood. 2014;124:2937–2947.
12. Zöller M. CD44, hyaluronan, the hematopoietic stem cell, and leukemia-initiating cells. Front Immunol. 2015;6:235.
13. Lee-Sayer SSM, Dougan MN, Cooper J, et al. CD44-mediated hyaluronan binding marks proliferating hematopoietic progenitor cells and promotes bone marrow engraftment. PLoS One. 2018;13:e0196011.
14. Evanko SP, Potter-Perigo S, Bollyky PL, Nepom GT, Wight TN. Hyaluronan and versican in the control of human T-lymphocyte adhesion and migration. Matrix Biol. 2012;31:90–100.
15. Goncharova V, Serobyan N, Iizuka S, et al. Hyaluronan expressed by the hematopoietic microenvironment is required for bone marrow hematopoiesis. J Biol Chem. 2012;287:25419–25433.
16. Matrosova VY, Orlovskaya IA, Serobyan N, Khaldoyanidi SK. Hyaluronic acid facilitates the recovery of hematopoiesis following 5-fluorouracil administration. Stem Cells. 2004;22:544–555.
17. Watanabe Y, Takeuchi K, Higa Onaga S, et al. Chondroitin sulfate *N*-acetylgalactosaminyltransferase-1 is required for normal cartilage development. Biochem J. 2010;432:47–55.
18. Takeuchi K, Yoshioka N, Higa Onaga S, et al. Chondroitin sulphate *N*-acetylgalactosaminyl-transferase-1 inhibits recovery from neural injury. Nat Commun. 2013;4:2740.
19. Yoshioka N, Miyata S, Tamada A, et al. Abnormalities in perineuronal nets and behavior in mice lacking CSGalNAcT1, a key enzyme in chondroitin sulfate synthesis. Mol Brain. 2017;10:47.
20. Ida-Yonemochi H, Morita W, Sugiura N, et al. Craniofacial abnormality with skeletal dysplasia in mice lacking chondroitin sulfate *N*-acetylgalactosaminyltransferase-1. Sci Rep. 2018;8:17134.
21. Igarashi M, Takeuchi K, Sugiyama S. Roles of CSGalNAcT1, a key enzyme in regulation of CS synthesis, in neuronal regeneration and plasticity. Neurochem Int. 2018;119:77–83.
22. Ushiki T, Kizaka-Kondoh S, Ashihara E, et al. Noninvasive tracking of donor cell homing by near-infrared fluorescence imaging shortly after bone marrow transplantation. PLoS One. 2010;5:e11114.
23. Ushiki T, Huntington ND, Glaser SP, et al. Rapid inflammation in mice lacking both SOCS1 and SOCS3 in hematopoietic cells. PLoS One. 2016;11:e0162111.
24. Izumikawa T, Koike T, Shiozawa S, Sugahara K, Tamura J, Kitagawa H. Identification of chondroitin sulfate glucuronyltransferase as chondroitin synthase-3 involved in chondroitin polymerization: chondroitin polymerization is achieved by multiple enzyme complexes consisting of chondroitin synthase family members. J Biol Chem. 2008;283:11396–11406.
25. Miyata S, Nadanaka S, Igarashi M, Kitagawa H. Structural variation of chondroitin sulfate chains contributes to the molecular heterogeneity of perineuronal nets. Front Integr Neurosci. 2018;12:3.
26. Nairn AV, Kinoshita-Toyoda A, Toyoda H, et al. Glycomics of proteoglycan biosynthesis in murine embryonic stem cell differentiation. J Proteome Res. 2007;6:4274–4387.
27. Johnson CE, Crawford BE, Stavridis M, et al. Essential alterations of heparan sulfate during the differentiation of embryonic stem cells to Sox1-enhanced green fluorescent protein-expressing neural progenitor cells. Stem Cells. 2007;25:1913–1923.
28. Gasimli L, Hickey AM, Yang B, et al. Changes in glycosaminoglycan structure on differentiation of human embryonic stem cells towards mesoderm and endoderm lineages. Biochim Biophys Acta. 2014;1840:1993–2003.
29. Ruffell B, Johnson P. Chondroitin sulfate addition to CD44H negatively regulates hyaluronan binding. Biochem Biophys Res Commun. 2005;334:306–312.
30. Zheng Z, Katoh S, He Q, et al. Monoclonal antibodies to CD44 and their influence on hyaluronan recognition. J Cell Biol. 1995;130:485–495.
31. Wairanowska M, Ladd S, Moscinski LC, et al. Modulation of hyaluronan production by CD44 positive glioma cells. Int J Cancer. 2010;127:532–542.
32. Ohtake Y, Li S. Receptors of chondroitin sulfate proteoglycans and CNS repair. Austin J Neurol Disord Epilepsy. 2015;2:1010.
33. van Galen P, Kreso A, Mbong N, et al. The unfolded protein response governs integrity of the haematopoietic stem-cell pool during stress. Nature. 2014;510:268–272.
34. Sigurdsson V, Miharada K. Regulation of unfolded protein response in hematopoietic stem cells. Int J Hematol. 2018;107:627–633.
35. Liu L, Zhao M, Jin X, et al. Adaptive endoplasmic reticulum stress signalling via IRE1α-XBP1 preserves self-renewal of haematopoietic and pre-leukaemic stem cells. Nat Cell Biol. 2019;21:328–337.
36. Essers MA, Offner S, Blanco-Bose WE, et al. IFNalpha activates dormant haematopoietic stem cells in vivo. Nature. 2009;458:904–908.
37. Kobayashi H, Butler JM, O'Donnell R, et al. Angiocrine factors from Akt-activated endothelial cells balance self-renewal and differentiation of haematopoietic stem cells. Nat Cell Biol. 2010;12:1046–1056.
38. Takagaki S, Yamashita R, Hashimoto N, et al. Galactosyl carbohydrate residues on hematopoietic stem/progenitor cells are essential for homing and engraftment to the bone marrow. Sci Rep. 2019;9:7133.
39. Wight TN, Kang I, Merrilees MJ. Versican and the control of inflammation. Matrix Biol. 2014;35:152–161.
40. Asada N, Takeishi S, Frenette PS. Complexity of bone marrow hematopoietic stem cell niche. Int J Hematol. 2017;106:45–54.
41. Wang T, Glover B, Hadwiger G, Miller CA, Martino OD, Welch JS. Smc3 is required for mouse embryonic and adult hematopoiesis. Exp Hematol. 2019;70. 70−84.e6.
42. Korpetinou A, Skandalis SS, Labropoulou VT, et al. Serglycin: at the crossroad of inflammation and malignancy. Front Oncol. 2014;3:327.

Online Supplementary Method

Isolation of BM stromal cells and endothelial cells

After isolating the femur and tibia, the central BM was collected by flushing out with a syringe and needle. Then, they were incubated in 4 mg/mL of collagenase type I (LS004194, Worthington, Lakewood, NJ, USA) in Dulbecco's Modified Eagle Medium (DMEM) at 37 ˚C with mild shaking and hemolyzed with ammonium-chloride-potassium (ACK) lysing buffer.

Flow cytometry Antibodies

Antibodies were sourced from Biolegend: c-Kit (2B8), Sca-1 (D7), Gr-1 (RB6-8C5), CD11b (M1/70), CD16/32(93), B220 (RA3-6B2), CD3 (17A2), CD44 (IM7), CD45.1 (A20), CD45.2 (104); eBioscience: CD34 (RAM34); and BD Biosciences: lineage antibody cocktail (CD3e, CD11b, CD45R/B220, Ter-119, Ly-6G and Ly-6c). To stain the RNA contents, Lineage-Sca-1+c-Kit+ (LSK) cells were incubated with 1 mg/mL Pyronin Y (Sigma Aldrich, St. Louis, MO, USA) at 37 ˚C for 20 min.

Flow cytometric analyses and cell sorting of bone marrow stromal cells and endothelial cells were performed using monoclonal antibodies recognizing the following antigens: Leptin receptor (BAF497), CD45 (30F11), PDGFRα (APA5), Sca1 (D7), CD31 (390), Ter119 (TER-119), CD51 (RMV-7), CD105 (MJ7/18), CD144 (BV13). These antibodies were purchased from BD Biosciences, eBioscience, BioLegend, TOMBO, and R&D Systems. Dead cells were removed by staining with 0.5 μg/ml propidium iodide (Sigma-Aldrich, St. Louis, MO, USA)

Immunofluorescence imaging

Isolated mouse femurs were immediately placed in an ice-cold 2% paraformaldehyde solution (PFA/PBS) and fixed under gentle agitation for 16 h. The samples were then incubated overnight in 15% and 30% sucrose for cryoprotection. Samples were embedded in OCT (Sakura, Tokyo, Japan) and frozen in cooled hexane. Frozen sections (7 μm) were generated using a cryostat (Cryostar NX70, Thermo Fisher Scientific, Waltham, MA, USA) using Kawamoto's tape method (Kawamoto, T. et al. Arch. Histol. Cytol. 2003). First, sections were blocked with staining buffer (10% normal donkey serum in TBS), treated with an Avidin/Biotin Blocking Kit (SP-2001, Vector Labs, Burlingame, CA, USA), followed by incubation with biotinylated anti-Lepin Receptor antibody (BAF497, R&D Systems, Minneapolis, MN, USA) and anti-Endomucin antibody (V.7C7, Santa Cruz Biotechnology, Dallas, TX, USA) in staining buffer overnight at 4 ˚C. For secondary staining, sections were incubated with streptavidin-AlexaFluor® 488 (S11223, Invitrogen, Carlsbad, CA, USA) and donkey anti-rat AlexaFluor® 594 (A-21209, Invitrogen) antibodies for 3 h at room temperature. Finally, sections were incubated with 1 μg/mL of DAPI/TBS for 10 min and mounted with ProLong Glass Antifade Mountant (P36982, Thermo Fisher Scientific) on a glass slide. Images of the sections were captured using a confocal microscope (Dragonfly, Andor Technology, Belfast, UK) with a 20× objective and processed using Fiji.

HPLC quantification

BM cells from tibia were flushed using a 25G needle and a 1 mL syringe filled with PBS; cells were filtered through a 70 μm nylon cell strainer (FALCON, Corning, New York, NY, USA) and were then centrifuged at 1500 rpm for 5 min at room temperature (RT). Cell pellets were resuspended in 2 mL ACK RBC lysis buffer (Gibco, Thermo Fisher Scientific, Waltham, MA, USA) and incubated for 5 min at RT. Cells were centrifuged and again washed twice under the same conditions. The final cell pellet was then frozen and stored at -80 ˚C.

Quantitative Real Time-PCR (qPCR)

Total RNA was isolated using the TRIzol RNA Isolation Reagent (Invitrogen, Carlsbad, CA, USA). The isolated RNA was reverse transcribed into complementary DNA (cDNA) with random primers using SuperScriptTM III (Invitrogen, Carlsbad, CA, USA). qPCR was carried out using the PowerUp SYBR green master mix (Thermo Fisher Scientific, Waltham, MA, USA) and was conducted on the StepOnePlus system (Applied Biosystems, Thermo Fisher Scientific, Waltham, MA, USA). qPCR was performed using the following primers: Gapdh: 5'-TTGTCAAGCTCATTTCCTGGT-3', 5'-TTACTCCTTGGAGGCCATGTA−3'; and CSGalNAcT1: 5' −TAAACAGCCCTGTGGAGAG−3', 5'GTCGAAATAGGACAAGTCGC−3'. Gene expression levels were calculated by the ΔCt method with GAPDH as endogenous control.

RNA Sequencing

Total RNA was extracted from WT and T1KO BM LSK cells using RNeasy® Plus Micro Kit (QIAGEN, Hilden, Germany) and cDNA was synthesized using the SMART-Seq v4 Ultra Low Input RNA Kit for Sequencing (Clontech, Palo Alto, CA, USA). ds-cDNA was fragmented using the S220 Focused-ultrasonicator (Covaris, Woburn, MA, USA), and then cDNA libraries were generated using the NEBNext® Ultra DNA Library Prep Kit (New England BioLabs, Beverly, MA, USA). Sequencing was performed using HiSeq1500 system (Illumina, San Diego, CA, USA) with a single-read sequencing length of 60 bp. The TopHat bioinformatics tool (version 2.0.13; with default parameters) was used to map to the reference genome (UCSC/mm10 or UCSC/hg19) with annotation data from iGenomes (Illumina, San Diego, CA, USA). Gene expression levels were quantified using the Cuffdiff program (Cufflinks version 2.2.1; with default parameters).

Online Supplementary Table 1. Upregulated and downregulated genes in LSK cells from T1KO mice compared to that of WT mice.

Upregulated Genes

Gene Symbol	Refseq ID	RPKM				average		log2((T1KOave+1)/(WTave+1))
		WT 1	WT 2	T1KO 1	T1KO 2	WT	T1KO	T1KO/WT
Atf3	NM_007498	0.315702	1.14467	0.220374	25.5997	0.79092714	3.79805435	3.00712721
Bc1	NR_038088, NR_038088_1	0	0	6.19291	0	0	2.034375967	2.034375967
Ccl3	NM_011337	37.5742	57.2096	32.0269	240.509	5.596693679	7.100851007	1.504157328
Ccl4	NM_013652	53.0755	56.1772	50.3496	277.556	5.797696539	7.365909457	1.568212918
Cd69	NM_001033122	11.778	14.7332	11.3081	46.7819	3.833456857	4.909053017	1.07559616
Cep85	NM_144527	7.96372	8.47974	24.2154	20.3398	3.205037426	4.540870414	1.335832988
Cldn5	NM_013805	2.06362	1.94536	7.32077	6.66819	1.58712012	2.999004197	1.411884077
Cxcl2	NM_009140	0	0.383234	0.0460491	7.38525	0.252920611	2.237456506	1.984535896
Dnd1	NM_173383	3.37399	2.61207	8.23926	9.23064	1.997483911	3.283173569	1.285689658
Ear12	NM_001012766	0.000237486	0.000477194	0.58307	2.00133	0.000515441	1.196732928	1.196217488
Egr1	NM_007913	131.993	191.46	78.5245	585.789	7.346305403	8.380057314	1.033751911
Erdr1	NM_133362	7.90141	9.44456	30.9739	38.2678	3.273961162	5.154650038	1.880688876
Fosb	NM_008036	5.09377	7.47548	5.2888	46.6754	2.864854707	4.753930732	1.889076025
Ier3	NM_133662	68.1224	77.5884	73.3682	270.2	6.206631504	7.432826653	1.22619515
Klf6	NM_011803	24.9276	34.7863	23.9349	138.083	4.947523563	6.357709461	1.410185898
Krtcap3	NM_027221	3.55094	4.28804	10.5808	10.4996	2.29850876	3.528596322	1.230087562
Ndufs5	NM_001030274	0.000744294	3.80668	0.000689388	14.3913	1.537898442	3.03491905	1.497020608
Nfkbiz	NM_001159394, NM_001159395, NM_030612	2.32494	3.26944	3.39763	25.8611	1.924932189	3.96618726	2.041255071
Nr4a1	NM_010444	5.49021	7.51692	4.26781	95.394	2.907576194	5.667634012	2.760057818
Pitx2	NM_001042502, NM_001042504, NM_001286942, NM_011098	2.19362	1.19293	4.87738	4.34072	1.429361545	2.487756443	1.058394898
Plk2	NM_152804	1.48708	1.65403	1.0664	10.2961	1.362079881	2.740118043	1.378038162
Ppp1r15a	NM_008654	30.1177	46.342	28.9736	190.44	5.293879914	6.79060003	1.496720116
Rasd1	NM_009026	2.50093	1.98683	4.59695	8.69791	1.697720451	2.934974996	1.237254545
Rgs1	NM_015811	29.4193	37.7402	27.1398	225.987	5.111855534	6.995070646	1.883215112
Socs3	NM_007707	5.45822	5.32127	8.45727	23.0597	2.675758358	4.066819827	1.39106147
Spry1	NM_001305440, NM_001305441, NM_001305442, NM_011896	14.2804	18.33	12.5593	56.7418	4.11313371	5.155852429	1.042718719
Trib1	NM_144549	1.51113	3.03228	1.85915	13.1949	1.710042671	3.092042486	1.381999816

Downregulated Genes

Gene Symbol	Refseq ID	RPKM				average		log2((T1KOave+1)/(WTave+1))
		WT 1	WT 2	T1KO 1	T1KO 2	WT	T1KO	T1KO/WT
Akr1b3	NM_009658	9.34814	4.28646	3.70677	1.27761	2.966670404	1.804132054	-1.16253835
Btg3	NM_001297747, NM_001297747_1, NM_009770	3.73466	1.24441	0.000326026	0.00032261	1.803034802	0.000467816	-1.802566986
Cd59a	NM_001111060, NM_007652	14.0161	13.9604	5.19839	5.3136	3.905760042	2.64523936	-1.260520682
Cdk5rap1	NM_025876	21.6331	17.5243	8.08179	7.54736	4.363079942	3.139891011	-1.223188931
Cma1	NM_010780	2.37092	0.551718	0.0940043	0	1.299431651	0.066264405	-1.233167246
Csgalnact1	NM_001252623, NM_172753	15.9831	15.3251	2.94508	4.32923	4.057805487	2.213239951	-1.844565536

(*continued on next page*)

Online Supplementary Table 1 (*Continued*)

Downregulated Genes

		RPKM				average		log2((T1KOave+1)/(WTave+1))
Gene Symbol	Refseq ID	WT 1	WT 2	T1KO 1	T1KO 2	WT	T1KO	T1KO/WT
Epx	NM_007946	0.0207807	8.65859	0	0	2.416754731	0	-2.416754731
Gm38670	NR_128568	173.731	189.36	0	0	7.512112295	0	-7.512112295
H2-Q8	NM_023124	9.71214	15.0448	2.14546	6.81675	3.74184123	2.454466772	-1.287374457
Moap1	NM_001142937, NM_022323	3.6591	1.88764	0.00827357	0.544936	1.915853571	0.35231196	-1.563541611
Prg2	NM_008920	0.44372	122.179	0.753768	0.989012	5.9614233	0.904110249	-5.057313051
Prg3	NM_016914	0	2.84202	0.0537605	0.332389	1.275609038	0.254684435	-1.020924603
Sap25	NM_001081962	2.27669	2.10709	0.209893	0.32538	1.674410934	0.342141106	-1.332269828
SlcUbl4a	NM_001278271, NM_001278272, NR_103489	0.827057	2.04113	0.277284	0	1.283384587	0.187314221	-1.096070366
Spib	NM_019866	0.119358	18.041	0.239676	6.55495	3.333449353	2.136622227	-1.196827126
Syce1	NM_001143765	1.32822	0.798152	0.0618846	0	1.044873889	0.04396359	-1.000910299
Tff2	NM_009363	1.68751	1.81699	0.390169	0	1.460611523	0.257112629	-1.203498893
Tpsb2	NM_010781	3.16329	0	0	0	1.36829063	0	-1.36829063
Akr1b3	NM_009658	9.34814	4.28646	3.70677	1.27761	2.966670404	1.804132054	-1.16253835
Btg3	NM_001297747, NM_001297747_1, NM_009770	3.73466	1.24441	0.000326026	0.00032261	1.803034802	0.000467816	-1.802566986
Cd59a	NM_001111060, NM_007652	14.0161	13.9604	5.19839	5.3136	3.905760042	2.64523936	-1.260520682
Cdk5rap1	NM_025876	21.6331	17.5243	8.08179	7.54736	4.363079942	3.139891011	-1.223188931
Cma1	NM_010780	2.37092	0.551718	0.0940043	0	1.299431651	0.066264405	-1.233167246
Csgalnact1	NM_001252623, NM_172753	15.9831	15.3251	2.94508	4.32923	4.057805487	2.213239951	-1.844565536
Epx	NM_007946	0.0207807	8.65859	0	0	2.416754731	0	-2.416754731

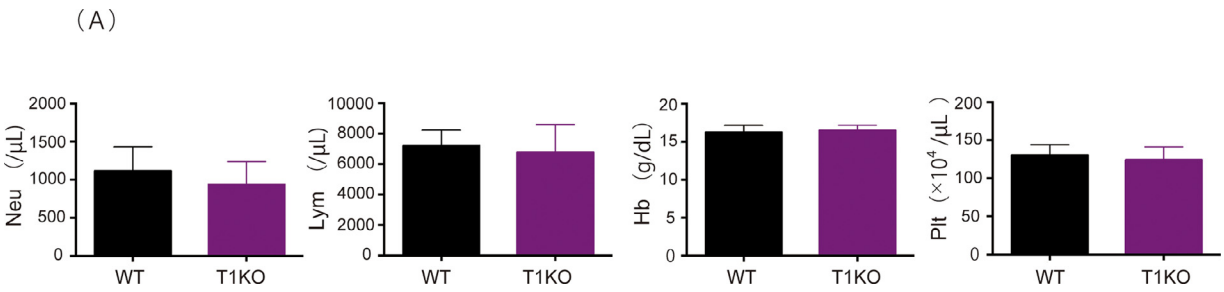

Online Supplementary Figure 1. PB cells of WT and T1KO did not show significant differences under steady state. **(A)** The numbers of PB cells (neutrophils, lymphocytes, Hb and platelets) of WT and T1KO mice under steady state (WT; n = 15, T1KO; n = 15). Data are represented as mean ± SD, * $P < .05$; ** $P < .01$; *** $P < .001$.

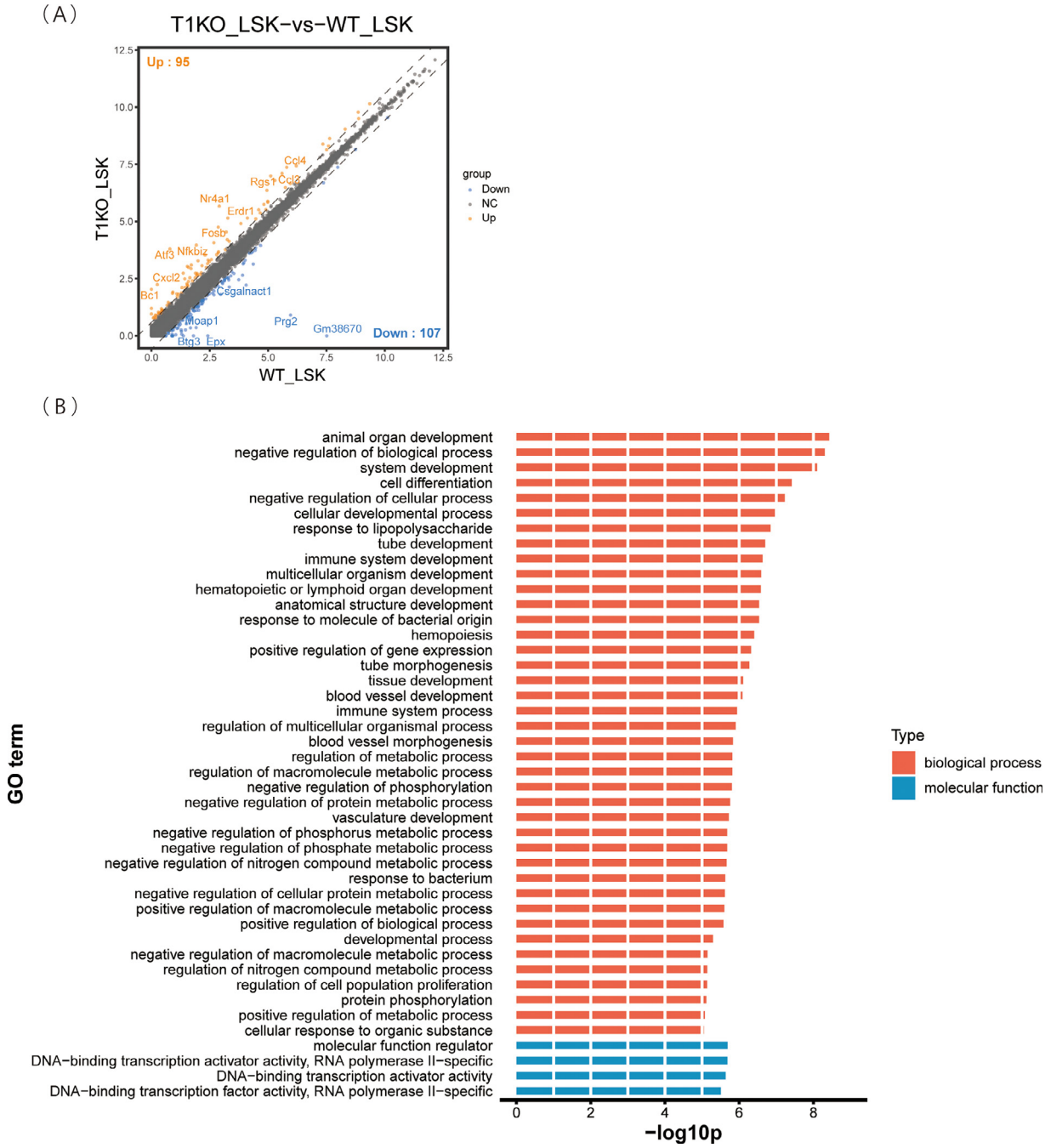

Online Supplementary Figure 2. GO analysis of the RNA-seq data shows enrichment of genes involved in various biological processes, including developmental and metabolic processes, among genes upregulated in T1KO LSK cells. **(A)** Scatter plots of gene sets (cut-off, fold-change ≥ 1.5). The x and y axes indicate the $\log_{10}$-scaled FPKM of the T1KO LSK and WT LSK groups, respectively. Gray dots represent genes with no change (NC) in expression. Orange and blue dots represent genes upregulated and downregulated in T1KO LSK cells, respectively (WT, n = 2; T1KO, n = 2). **(B)** Bar graph of GO terms in which genes enriched in T1KO LSK cells are mainly involved. The x axis indicate $\log_{10}$-scaled P values.